Human Molecular Genetics, 2012, Vol. 21, No. 6 **1272–1286**
doi:10.1093/hmg/ddr557
Advance Access published on November 25, 2011

A meckelin–filamin A interaction mediates ciliogenesis

Matthew Adams[1], Roslyn J. Simms[3], Zakia Abdelhamed[1], Helen R. Dawe[4], Katarzyna Szymanska[1], Clare V. Logan[1], Gabrielle Wheway[1], Eva Pitt[2], Keith Gull[5], Margaret A. Knowles[2], Edward Blair[6], Sally H. Cross[7], John A. Sayer[3] and Colin A. Johnson[1,*]

[1]Ciliopathy Research Group, Section of Ophthalmology and Neurosciences and [2]Section of Experimental Oncology, Leeds Institute of Molecular Medicine, University of Leeds, Leeds LS9 7TF, UK, [3]Institute of Human Genetics, International Centre for Life, Newcastle University, Newcastle-upon-Tyne NE1 3BZ, UK, [4]Biosciences, College of Life and Environmental Sciences, Geoffrey Pope Building, University of Exeter, Stocker Road, Exeter EX4 4QD, UK, [5]Sir William Dunn School of Pathology, University of Oxford, South Parks Road, Oxford OX1 3RE, UK, [6]Department of Clinical Genetics, Churchill Hospital, Old Road, Headington, Oxford OX3 7LJ, UK and [7]MRC Human Genetics Unit, Western General Hospital, Crewe Road, Edinburgh EH4 2XU, UK

Received September 29, 2011; Revised November 18, 2011; Accepted November 22, 2011

***MKS3*, encoding the transmembrane receptor meckelin, is mutated in Meckel–Gruber syndrome (MKS), an autosomal-recessive ciliopathy. Meckelin localizes to the primary cilium, basal body and elsewhere within the cell. Here, we found that the cytoplasmic domain of meckelin directly interacts with the actin-binding protein filamin A, potentially at the apical cell surface associated with the basal body. Mutations in *FLNA*, the gene for filamin A, cause periventricular heterotopias. We identified a single consanguineous patient with an MKS-like ciliopathy that presented with both MKS and cerebellar heterotopia, caused by an unusual in-frame deletion mutation in the meckelin C-terminus at the region of interaction with filamin A. We modelled this mutation and found it to abrogate the meckelin–filamin A interaction. Furthermore, we found that loss of filamin A by siRNA knockdown, in patient cells, and in tissues from *Flna*^{Dilp2} null mouse embryos results in cellular phenotypes identical to those caused by meckelin loss, namely basal body positioning and ciliogenesis defects. In addition, morpholino knockdown of *flna* in zebrafish embryos significantly increases the frequency of dysmorphology and severity of ciliopathy developmental defects caused by *mks3* knockdown. Our results suggest that meckelin forms a functional complex with filamin A that is disrupted in MKS and causes defects in neuronal migration and Wnt signalling. Furthermore, filamin A has a crucial role in the normal processes of ciliogenesis and basal body positioning. Concurrent with these processes, the meckelin–filamin A signalling axis may be a key regulator in maintaining correct, normal levels of Wnt signalling.**

INTRODUCTION

Meckel–Gruber syndrome (MKS) is a lethal inherited developmental disorder characterized by a triad of clinical features that are renal cystic dysplasia, hepatic developmental defects and severe neurodevelopmental anomalies including neural tube defects such as occipital encephalocele, anencephaly and exencephaly. MKS is a ciliopathy, caused by mutations in genes encoding proteins that are components of the primary cilium and basal body (1–4). MKS is genetically heterogenous and displays marked pleiotropy, in that mutations in most of the eight recently identified genes (*MKS1*, *MKS2/TMEM216*, *MKS3/TMEM67*, *CEP290*, *RPGRIP1L*, *CC2D2A*, *NPHP3*, *TCTN2*) cause a range of phenotypes (1–11). *MKS3/TMEM67* is a gene mutated in patients with either MKS or the related ciliopathy, Joubert syndrome, and encodes meckelin (transmembrane protein 67). Meckelin is a 995 amino-acid transmembrane protein with structural similarity to Frizzled receptors (3,12).

*To whom correspondence should be addressed at: Department of Ophthalmology and Neurosciences, Leeds Institute of Molecular Medicine, Wellcome Trust Brenner Building, St. James's University Hospital, Leeds LS9 7TF, UK. Tel: +44 113 343 8443; Fax: +44 113 343 8603; Email: c.johnson@leeds.ac.uk

Meckelin consists of an extracellular N-terminal domain, three to seven predicted transmembrane regions, and an intracellular C-terminal region containing a coiled-coil domain (3) (Fig. 1A and Supplementary Material, Fig. S1A). Although meckelin localizes to the membrane of the primary cilium and the ciliary transition zone (13), it also has a non-ciliary distribution (Fig. 1B and Supplementary Material, Fig. S2C). Early in ciliogenesis, non-ciliary meckelin interacts directly with the actin-binding forms of nesprin-2 and can be associated with actin-based projections such as filopodia and microspikes (14). Meckelin also interacts with MKS1 and TMEM216, both also mutated in MKS. Notably, meckelin, nesprin 2, MKS1 and TMEM216 are all required for centrosome migration to the apical cell surface during ciliogenesis, a crucial step leading to the subsequent formation of the primary cilium (4,6,14,15).

Filamin A (ABP280, actin-binding protein 280, or filamin 1; Fig. 1C) is an actin-binding protein that belongs to the filamin family, which includes filamins B and C. Filamins are large, multifunctional cytoplasmic proteins which mediate positioning of the actin cytoskeleton (16,17). Mutations in *FLNA*, the gene encoding filamin A, cause several human X-linked disorders (18–20). Loss-of-function mutations resulting in abnormal mRNA splicing or early truncation of the protein cause periventricular heterotopia (PVH) (20), an X-linked disorder with variable presentation in female patients and embryonic lethality in males (21). Most female patients develop vascular disorders and seizures caused by neuronal cell migration defects during development of the cerebral cortex. This leads to formation of nodules in the ependymal layer of the cerebral ventricles (20).

In the present study, we demonstrate that the C-terminal cytoplasmic region of meckelin interacts with filamin A. Loss of either filamin A or meckelin, by siRNA knockdown or in immortalized patient fibroblasts, cause similar cellular phenotypes. These include defects in basal body positioning and ciliogenesis, aberrant remodelling of the actin cytoskeleton and deregulation of RhoA activity, and deregulation of canonical Wnt signalling. Basal body positioning and ciliogenesis are also defective in the neuroepithelium during neocortex formation in mouse embryos deficient for filamin A. Furthermore, we confirm *in vivo* the interaction between filamin A and meckelin by the analysis of morphant phenotypes following morpholino knockdown in zebrafish embryos. To further prove the importance of the meckelin–filamin A axis, we modelled an unusual pathogenic mutation (c.2754_2756delCTT p.I918_F919del) in the C-terminal region of meckelin that interacted with filamin A. This mutation was identified in a patient with the clinical features of MKS, in addition to focal glial heterotopia in the cerebellum, a highly unusual feature in MKS. We found that this mutation caused abrogation of the meckelin interaction with filamin A, ciliogenesis defects and negative modulation of Wnt signalling.

RESULTS

Filamin A interacts with the meckelin C-terminal domain and localizes to the basal body

We first characterized a rabbit polyclonal anti-meckelin antibody raised against the meckelin C-terminus (Ct Ab; amino acids 982–995; Fig. 1A and Supplementary Material, Fig. S1A) (6). By western blotting, the antibody recognized full-length meckelin (110 kDa), shorter meckelin isoforms (Supplementary Material, Fig. S2A) and full-length haemoagglutinin (HA)-tagged meckelin (Supplementary Material, Fig. S2B). A second anti-meckelin antibody against the N-terminus (Nt Ab; amino acids 100–113; Fig. 1A and Supplementary Material, Fig. S1A) also recognized full-length meckelin and shorter isoforms (Supplementary Material, Fig. S2A). Both antibodies demonstrated a strong meckelin localization to the basal body and the peribasal body area (Fig. 1B) (6,14). The 'Nt Ab' antibody also demonstrated localization to the proximal regions of the primary cilium consistent with a previously described localization to the transition zone (13) (Fig. 1B; arrow**)**. The 'Ct Ab' antibody also showed non-ciliary meckelin at the apical cell surface (Fig. 1B; lower panels) and a vesicle-like pattern at basolateral surfaces and basal surfaces (Supplementary Material, Fig. S2C). The vesicle-like distribution suggested an association of non-ciliary meckelin with elements of the actin cytoskeleton (Supplementary Material, Fig. S2C) and implied diverse roles for meckelin at the primary cilium and throughout the cell.

To identify proteins that interact with meckelin, the C-terminal region of meckelin (amino acids D761–Y925, containing the coiled-coil motif) was used as a bait fragment in a GAL4 fusion construct for a yeast-2-hybrid (Y2H) screen against preys in a human foetal brain cDNA library (see Ref. 14 for more details of Y2H). Filamin A (amino acids T2171–K2339; Fig. 1C and Supplementary Material, Fig. S1B) was identified as a potential interacting partner. Filamin A has two hinge regions: one between filamin A repeats 15 and 16 and the second between repeats 23 and 24, with a dimerization domain at repeat 24 (Fig. 1C). The meckelin-interacting domain was between the first hinge and dimerization domain of filamin A (*FLNA* repeats 20–22). This region of filamin A binds to several ligands implicated in actin remodelling (17,22–24).

To confirm that meckelin interacts with filamin A, immunoprecipitations (IPs) were performed on whole-cell extracts (WCEs) from confluent ciliated HEK293 cells. IP with affinity-purified anti-meckelin Ct ('Ct Ab') antibody, followed by immunoblotting with an anti-filamin A monoclonal antibody (MAb), indicated an interaction between endogenous meckelin and filamin A (Fig. 1D). Furthermore, we also detected an interaction between the basal body protein MKS1 and filamin A (Fig. 1D), a finding consistent with an interaction of MKS1 (2) with meckelin (6), suggesting an MKS protein–filamin A complex. Meckelin Ct (amino acids E756–I995) was also sub-cloned and bacterially expressed as a GST fusion protein. GST pull-down experiments were performed using GST-meckelin-Ct and GST alone on WCEs, followed by immunoblotting with an anti-filamin A antibody. This also demonstrated a biochemical interaction between endogenous filamin A and meckelin Ct, confirming the Y2H screen results (Fig. 1D).

Filamin A co-localized with MKS1 at the apical cell surface in polarized confluent IMCD3 cells (Fig. 1E). The pattern of filamin A was consistent with a basal body/transition zone localization as demonstrated for both meckelin (Fig. 1B) and MKS1 (6). In the main cell body, we also demonstrated a localization of non-ciliary meckelin with filamin A at the

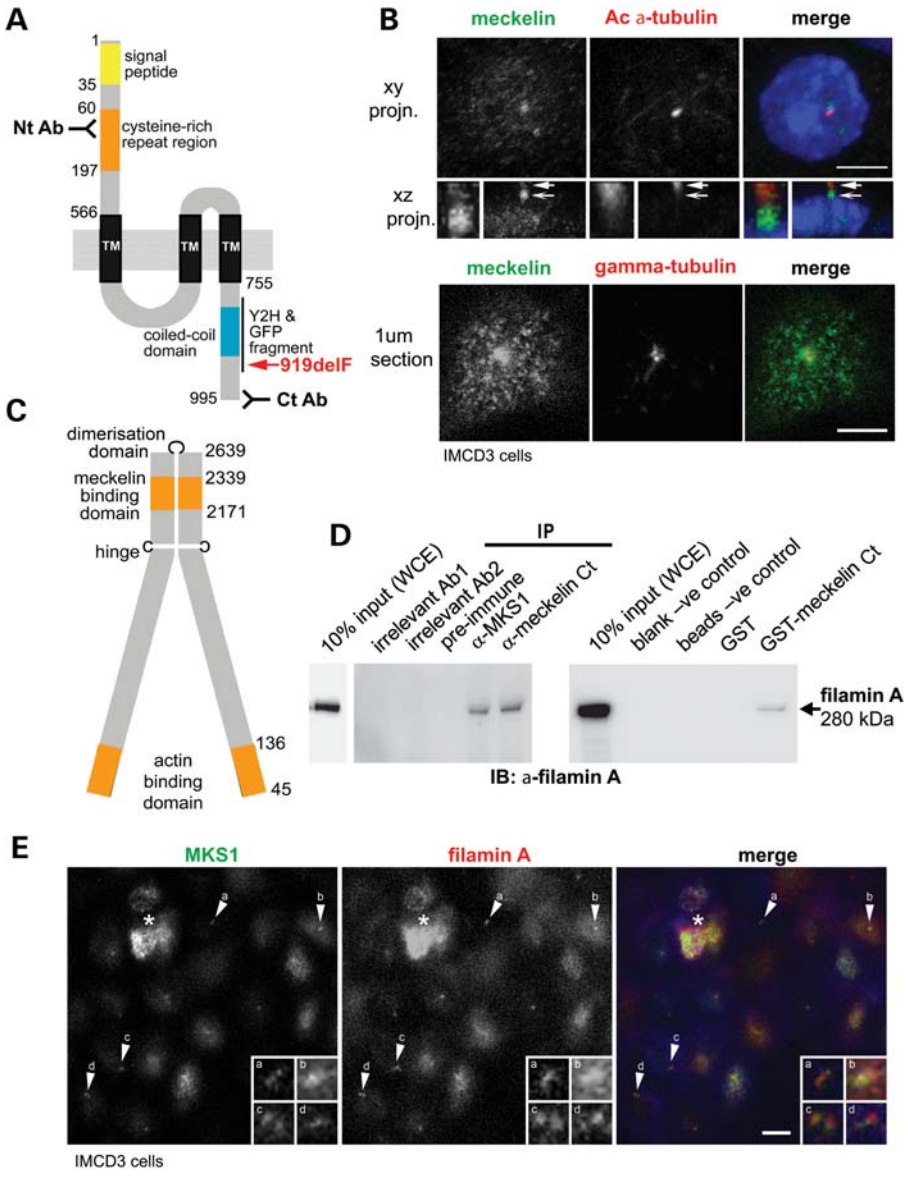

Figure 1. Meckelin localizes to the primary cilium and basal body and interacts with filamin. (**A**) Domain structure of meckelin showing the locations of predicted signal peptide, cysteine-rich repeat region, a region containing potential three to seven transmembrane domains (TM) and a coiled-coil domain. Indicated are the locations of epitopes for two anti-meckelin antibodies ('Nt Ab' and 'Ct Ab'), the C-terminal region used for a Y2H bait fragment and a meckelin Ct-GFP construct, and the pathogenic MKS in-frame deletion mutation p.919delF (red). Numbering indicates the amino-acid residue. (**B**) Upper panels: Co-immunostaining and confocal microscopy of a ciliated mouse IMCD3 epithelial cell for meckelin (using the Nt Ab; green in merged image) and acetylated (Ac)-α-tubulin antibody (red) showing co-localization of meckelin isoforms at the cilium. A confocal $x–y$ projection (planar projn.) and $x–z$-side projection are shown. Enlarged insets (white frames) show detail of localization at the proximal region of the cilium (arrow) and the basal body (barbed arrow). Nuclear localization of 4′,6-diamidino-2-phenylindole (DAPI) is shown in blue. Scale bar, 5 μm. Lower panels: 1 μm confocal section of the apical cell surface following co-immunostaining for meckelin Ct (green) and γ-tubulin (red). At the apical surface, meckelin had a punctate distribution and strong peribasal body accumulation. Scale bar, 5 μm. (**C**) Domain structure of filamin A showing meckelin-binding domain, actin-binding domain, dimerization domain and hinge. Numbering indicates the amino-acid residue. (**D**) Left panel: IP of endogenous filamin A (size 280 kDa) from confluent HEK293 WCE with anti-meckelin Ct ('Ct Ab') and anti-MKS1 but not by pre-immune serum-negative control or two irrelevant antibodies (Ab1 and Ab2). Right panel: pull-down of filamin A from WCE by GST-tagged meckelin Ct but not by GST alone, or blank and beads only negative (−ve) controls. Western immunoblotting (IB) was with an anti-filamin A MAb. Ten percent of total input WCE is indicated. (**E**) Co-immunostaining and confocal microscopy of a ciliated mouse IMCD3 epithelial cell for MKS1 (a basal body marker; green in merged image) and filamin A (red) showing localization of filamin A to the basal body and apical cell surface. A 2 μm apical section is shown. Enlarged insets (white frames, labelled a–d) show detail of localization at the basal body (arrows a–d). Scale bar, 5 μm. The asterisk indicates a cell above the monolayer.

basolateral cell surfaces consistent with an association of meckelin with the actin cytoskeleton (Supplementary Material, Fig. S2C).

The filamins are a family of actin-binding proteins, so we next analysed the effect of meckelin loss on the actin cytoskeleton. We silenced *Mks3* expression using siRNA duplexes,

which we validated to cause loss of protein expression (Supplementary Material, Fig. S2D) (6,14). Next, we determined the subcellular distribution and integrity of the actin cytoskeleton. In negative control scrambled siRNA-transfected cells, the actin cytoskeletal network was intact, but in *Mks3*-silenced cells, basal and basolateral actin was lost alongside extensive disruption of cell–cell contacts (Supplementary Material, Fig. S2E and F). Ciliogenesis was also disrupted, as expected from our previous studies (6,14) alongside disruption of the actin cytoskeleton (Supplementary Material, Fig. S2F). This suggested that anchoring of actin at the cell cortex during ciliogenesis could be mediated by meckelin, specifically at the basal and basolateral cell surfaces where actin is crucial in maintaining cell–cell contacts.

A pathogenic *MKS3* mutation disrupts the meckelin–filamin A interaction, leads to loss of cilia formation and reduces RhoA activity

Khaddour *et al*. (25) identified that most *MKS3* mutations are in exons 1–18 ($n = 11/12$) and are not in the intracellular C-terminal domain of meckelin that interacted with filamin A. We identified an unusual homozygous pathogenic deletion mutation in *MKS3*, c.2754_2756delCTT p.I918_F919del (919delF) (K. Szymanska and C.A. Johnson, personal communication), predicted to result in the in-frame deletion of phenylalanine residue F919 in the cytoplasmic (C-terminal) region of meckelin that interacts with filamin A (Fig. 1A and Supplementary Material, Fig. S1A). This mutation was identified in a patient with an MKS-like ciliopathy with occipital encephalocele, hydrocephalus, cystic kidneys and ductal plate malformation in the liver. The hydrocephaly was distinguished by moderate dilatation of the left and right lateral ventricles and fourth ventricle. However, in addition to the MKS clinical features, this patient also presented with focal glial heterotopias of the cerebellum, which are an unusual association with MKS. Since *FLNA* mutation can lead to periventricular heteroptopia, a defect of neuronal migration, we modelled the *MKS3* 919delF mutation to determine the functional consequences of this mutation.

First, we assessed the effect of the *MKS3* 919delF mutation on cilia formation and transfected fibroblasts which lacked meckelin expression (14) with an empty HA vector, or vectors encoding either full-length HA-wild-type meckelin or HA-919delF mutant meckelin (Fig. 2A). When transfected with the empty vector, 10% of cells were ciliated, but when transfected with wild-type meckelin 29% of cells were ciliated ($P < 0.01$) demonstrating a partial rescue of the ciliopathy phenotype. However, when transfected with 919delF mutant meckelin, this rescue did not occur and only 8% of cells were ciliated (Fig. 2A and B). This confirmed that the *MKS3* 919delF mutation causes a defect in ciliogenesis.

We then performed IPs from transfected WCEs with affinity-purified anti-meckelin 'Ct Ab' antibody to pull down endogenous and transfected meckelin. In cells transfected with wild-type meckelin, we confirmed the meckelin–filamin A interaction (Fig. 2C). However, in cells transfected with mutant F918del HA-meckelin, the meckelin–filamin A interaction was lost (Fig. 2C). In parallel experiments, two different anti-HA antibodies (either a rabbit polyclonal or a mouse monoclonal) were used to pull down transfected epitope-tagged meckelin. These co-immunoprecipitated endogenous filamin A with wild-type meckelin, but this interaction was diminished with the mutant F919del HA-meckelin (Fig. 2C).

We have shown previously that loss of expression of two MKS genes, *MKS3/TMEM67* and *MKS2/TMEM216* (by either pathogenic mutations or RNAi), causes hyperactivation and mislocalization of RhoA (4,14). RhoA is a member of the small GTPase family implicated in many signalling processes (26). Therefore, we next analysed the 919delF mutation in the context of RhoA activity. Over-expression of wild-type HA-meckelin in IMCD3 cells had no effect on RhoA activation as measured in a pull-down assay, but mutant F919del HA-meckelin, which negates the meckelin–filamin A interaction (Fig. 2C), abolished almost all activation of RhoA (Fig. 2D). Thus, our results from Y2H, GST pull-down and IP demonstrated a direct biochemical interaction between the intracellular C-terminal region of meckelin (meckelin Ct) and filamin A which is lost when *MKS3* has a mutation in the interacting domain.

Filamin A mediates migration of the centrosome to the apical cell surface during ciliogenesis

We have previously shown that siRNA-mediated loss of meckelin prevented the correct migration of the centrosome to the apical cell surface and subsequent ciliogenesis (6,14). We therefore asked whether filamin A is also required for the correct positioning of the basal body during ciliogenesis.

In immortalized dermal fibroblasts taken from a female patient with PVH caused by a heterozygous *FLNA* frameshift mutation, c.1587delG p.K529fs, we immunostained with anti-filamin A antibodies and confirmed the loss of filamin A expression. *FLNA* is on chromosome Xq28, so cells displayed an apparent mosaic pattern due to random X-chromosome inactivation (Fig. 3A, Supplementary Material, Fig. S3A). We then correlated filamin A expression with the presence of primary cilia, alteration in the distribution of meckelin and defects in basal body position. We confirmed that filamin A loss impaired but did not completely prevent ciliogenesis (Fig. 3B).

The distribution of non-ciliary meckelin Ct was largely undisrupted in PVH cells (Fig. 3A). However, analysis of basal body positioning showed that in filamin A null cells, the basal body was retained in the mid-portion of the cell, compared with a predominantly apical location in filamin A-positive cells (Fig. 3A and C). In contrast, further immunostaining of the PVH fibroblasts demonstrated that neither the actin cytoskeleton nor filamin B distribution was disrupted in filamin A null cells when compared with filamin A-positive cells (Supplementary Material, Fig. S3A).

We next silenced *Flna* expression using siRNA duplexes, validated loss of protein expression (Supplementary Material, Fig. S3B) and determined the presence of the primary cilium and basal body position in IMCD3 cells (+72 h after confluency). In negative control scrambled siRNA-transfected cells, the proportion of ciliated cells and basal body position were at expected levels, but in *Flna*-silenced cells, ciliogenesis was impaired and basal body positioning was disrupted

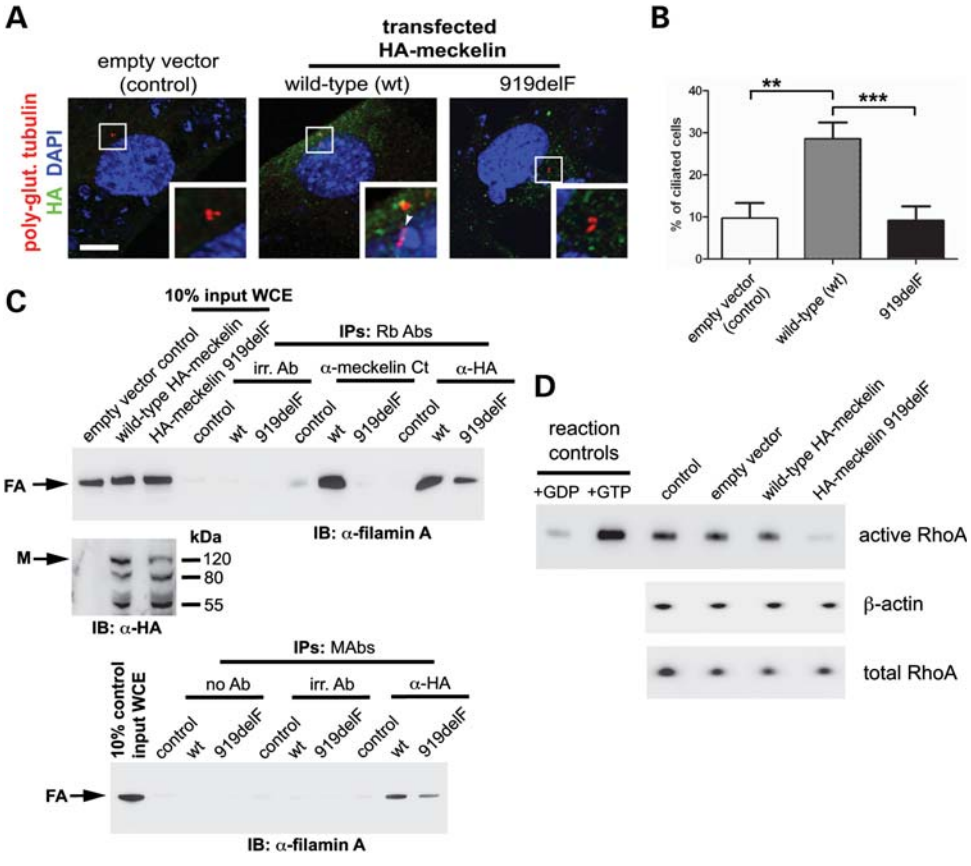

Figure 2. A pathogenic *MKS3* mutation causes loss of cilia formation and disrupts the meckelin–filamin A interaction. (**A**) *MKS3*-null fibroblasts (12) were transfected with empty vector negative control (control), wild-type HA-meckelin (wt) or p.F919del mutant HA-meckelin (919delF) constructs and were immunostained for HA (green), polyglutamylated tubulin and DAPI. Cells transfected with wt-HA-meckelin had a primary cilium (indicated by an arrowhead in enlarged inset, white border), whereas in cells transfected with p.F919del mutant HA-meckelin, the primary cilium was absent (enlarged inset, white border). Scale bar, 5 μm. (**B**) Graph quantifying the proportion of ciliated cells in *MKS3*-null fibroblasts (14) transfected with empty vector negative control (control), wild-type HA-meckelin (wt) or p.F919del mutant HA-meckelin (919delF). Ten percent of control cells were ciliated, 29% of cells transfected with wild-type HA-meckelin were ciliated and 9% of cells transfected with p.F919del mutant HA-meckelin were ciliated. $^{**}P < 0.01$; $^{***}P < 0.001$ (Student's *t*-test). For each transfected cell population, a minimum of 500 cells were counted from 10 separate fields of view. (**C**) IP of endogenous filamin A by wild-type meckelin HEK293 cells were transfected with empty vector negative control (control), wild-type HA-meckelin (wt) or p.F919del mutant HA-meckelin (919delF) constructs. Top panel: 10% of total input WCE for each IP is indicated. Affinity-purified 'Ct Ab' anti-meckelin antibody against the C-terminus and anti-HA rabbit polyclonal (Rb Abs) against epitope-tagged wild-type HA-meckelin preferentially pull-down endogenous filamin A (arrow). Expression of the p.F919del mutant HA-meckelin (919delF) abrogated or prevented interaction with filamin A. IP for empty vector negative control (control), no antibody (no Ab) control and irrelevant antibodies (irr. Ab.) did not pull-down filamin A. Middle panel: expression of HA-tagged proteins determined by immunoblotting (IB) with Rb Ab anti-HA full-length meckelin (size 110 kDa) is indicated (arrow). Other smaller isoforms (80 and 55 kDa) are also recognized (refer to Supplementary Material, Fig. S2B). Bottom panel: anti-HA mouse MAbs against epitope-tagged wild-type HA-meckelin preferentially pulls down endogenous filamin A (arrow). (**D**) Rho activation pull-down assay HEK293 cells transfected with empty vector, wild-type HA-meckelin and p.F919del mutant HA-meckelin constructs. Expression of mutant meckelin caused a decrease in levels of activated RhoA-GTP when compared with wild-type meckelin, empty vector and a transfection reagent only negative control (control). Total RhoA and β-actin are shown as loading controls. A positive control for the assay (+GTP; loading with non-hydrolysable GTPγS) and a negative control (+GDP; loading with GDP) are also shown.

(Fig. 3D and E). In summary, our findings demonstrated that filamin A is necessary for optimal cilia formation and for correct positioning of the basal body in patient-derived fibroblasts and IMCD3 cells. This suggests that some of the features of PVH caused by *FLNA* mutation may be due to impaired ciliogenesis.

The filamins have overlapping functions (19,24,27) and we observed that the distribution of filamin B was unaffected in filamin A null PVH fibroblasts (Supplementary Material, Fig. S3A). Therefore, we next looked for an association of filamin B with the basal body or cilium. In polarized ciliated IMCD3 cells, we immunostained with an anti-MKS1 antibody, to mark the position of the basal body, and an anti-filamin B antibody. We identified a localization of filamin B to either the basal body or proximal regions of the cilium (Supplementary Material, Fig. S3C) which indicted a potential role for other filamins in ciliogenesis.

Functional consequences of *MKS3* mutation or *FLNA* mutation in patients' cells

Perturbation of canonical Wnt signalling is implicated in the pathogenesis of ciliopathies (28,29). Therefore, to assess functional consequences of cilia loss due to *FLNA* or *MKS3* mutation, we tested whether Wnt activity was deregulated in appropriate patient-derived fibroblasts. Upon stimulation

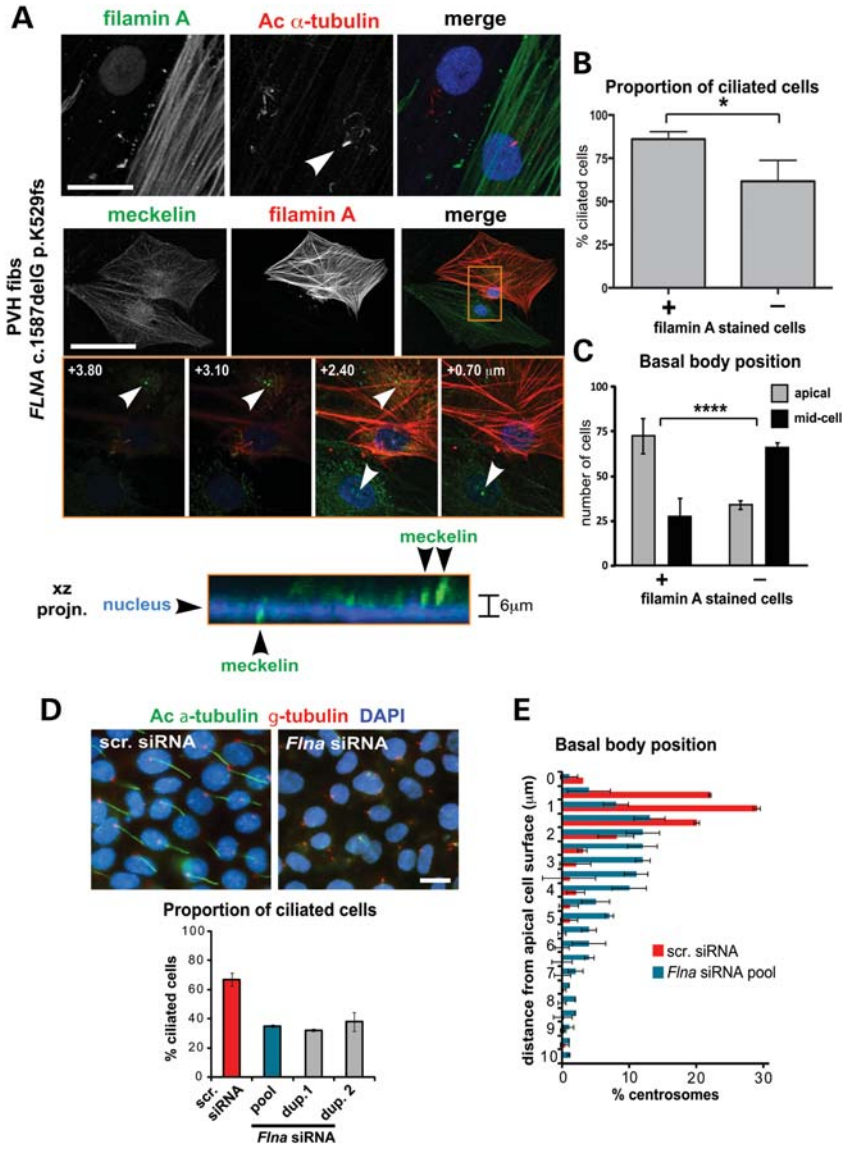

Figure 3. Defects in basal body positioning and ciliogenesis following loss of filamin A. (**A**) Co-immunocytostaining and confocal microscopy of serum-starved immortalized dermal fibroblasts (fibs) from a female patient with PVH carrying the *FLNA* frameshift mutation c.1587delG p.K529fs. Upper panel: staining for filamin A (green) and acetylated (Ac) a-tubulin (red). A primary cilium in the filamin A-positive staining cell is indicated (arrowhead). Middle panel: staining for meckelin Ct (green) and filamin A (red), with insets (orange frame), showing confocal z-sections at the indicated heights (μm) above the basal substrate (scale bars, 10 μm). Lower panel: x–z projection of inset (orange frame) showing position of meckelin (green) at the basal body in relation to the nucleus (DAPI; blue). The difference in relative basal body heights is indicated to the right of the panel. (**B**) Bar graph quantifying the proportion of ciliated cells in filamin A-positive and null PVH fibroblasts. Sixty-two percent of filamin A null cells ($n = 176$) had cilia when compared with 88% of filamin A-positive cells ($n = 174$, error bars = SEM, $^{*}P < 0.01$, Student's t-test). (**C**) Bar graph quantifying the position of the basal body in filamin A-positive and null PVH fibroblasts. In filamin A null cells, the basal body was retained in the mid-portion of the cell (66.1%; $n = 125$, defined as present in the lowermost three-quarters of z-sections), whereas the majority of filamin A-positive cells had an apical basal body (72.4%; $n = 133$, error bars = SEM, $^{****}P < 10^{6}$, χ^2- test). (**D**) Impairment of ciliogenesis in serum-starved IMCD3 cells following transfection with mouse filamin A (*Flna*) siRNA pooled duplexes (dup.) but not scrambled (scr.) control. Merged images show localization of cilia (acetylated a-tubulin, green), basal bodies (g-tubulin, red) and nuclei (DAPI, blue). Scale bar, 5 μm. Bar graph quantifies the percentage of ciliated cells following transfection with the indicated siRNAs. Values shown are means for $n = 120$ or greater, for three independent replicates with error bars indicating SEM. (**E**) Bar graph quantifying the percentage of centrosomes measured at the indicated distances from the apical cell surface in IMCD3 cells, following transfection with either scrambled (scr.) control siRNA (blue bars) or *Flna* siRNA pooled duplexes (red bars). Values shown are means for $n = 1000$ or greater, for three independent replicates with error bars indicating SEM.

with conditioned media containing Wnt3A, a ligand for the canonical Wnt signalling pathway, *MKS3*-mutated patient fibroblasts had aberrant hyperactivation of canonical Wnt signalling (over 5-fold basal levels) when compared with normal control fibroblasts (Fig. 4A and Supplementary Material, Fig. S4). Treatment with Wnt5A, a ligand for the non-canonical Wnt signalling pathway, had no effect on activation, but, as expected, suppressed the activation by Wnt3A (Fig. 4A). Co-expression of wild-type HA-meckelin inhibited canonical Wnt signalling and partially rescued the aberrant response to Wnt3A by the *MKS3*-mutated cells. Mutant F919del HA-meckelin had a further inhibitory effect on canonical

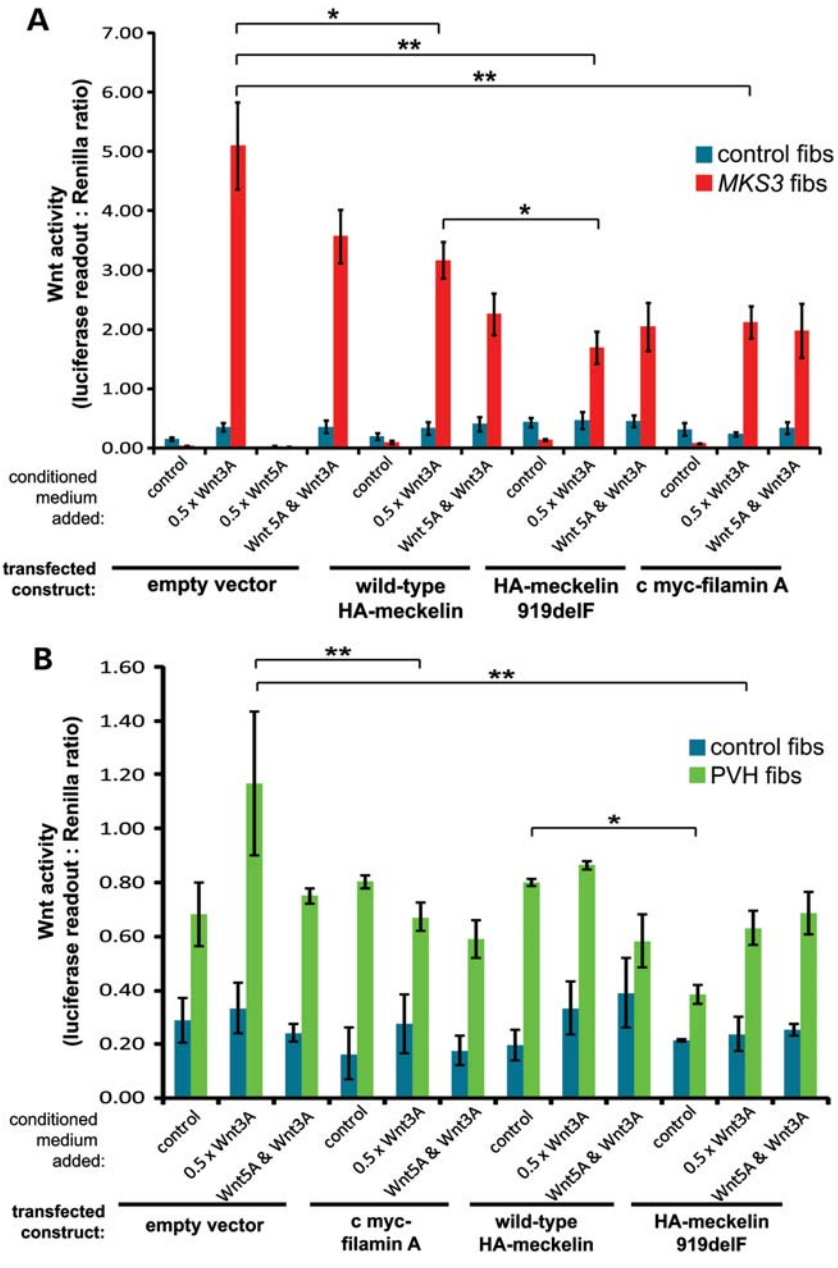

Figure 4. Loss of meckelin or filamin A causes deregulation of Wnt signalling. (**A**) TopFlash assays to measure levels of activated β-catenin, and hence canonical Wnt signalling, following co-transfection of immortalized normal control (control fibs, blue bars) and *MKS3*-mutated dermal fibroblasts (*MKS3* fibs, red bars; see Fig. 3C) with reporter constructs and empty vector, wild-type HA-meckelin, p.F919del mutant HA-meckelin constructs and c myc-filamin A, as indicated. The empty vector results combine the data from transfections with pCMV-HA and pCMV-c myc. Activity is expressed as ratios of luciferase reporter construct expression, normalized for loading by measurement of a *Renilla* construct expression. The responses are shown to 0.5 × L cell control conditioned media (control), and conditioned media containing expressed Wnt3A and/or Wnt5A. Values shown are means of at least four independent replicates, with error bars indicating SEM. Statistical significance of pair-wise comparisons are shown ($^{*}P < 0.01$ and $^{**}P < 0.001$, Student's *t*-test). (**B**) TopFlash reporter assays as in (A) for control fibroblasts (control fibs, blue bars) and *FLNA*-mutated fibroblasts (*FLNA* fibs, green bars). Values shown are means of three independent replicates. Statistical significance of pair-wise comparisons are shown ($^{*}P < 0.05$, error bars = SEM, $^{**}P < 0.01$, Student's *t*-test).

Wnt signalling, suggesting a possible gain-of-function effect for the F919del mutation. Co-expression of full-length filamin A alone also had a inhibitory effect on the aberrant canonical Wnt signalling in *MKS3* fibroblasts, suggesting that it could mediate the correct response of meckelin during Wnt signalling.

PVH *FLNA*-mutated fibroblasts also had mild perturbation of canonical Wnt signalling in response to activation by Wnt3A, which was partially rescued by co-expressed filamin A (Fig. 4B). Mutant F919del HA-meckelin also had an inhibitory effect on the aberrant canonical Wnt signalling in PVH fibroblasts, again suggesting that the F919del mutation has a gain-of-function effect. These responses are consistent with the primary cilium mediating correct Wnt signalling and suggest that Wnt signalling may be deregulated in ciliopathies.

Zebrafish embryo morphants for *mks3* reiterate features of MKS and interact with *flna* morphants to produce severe ciliopathy developmental defects

Following our *in vitro* findings, we next investigated whether the meckelin–filamin A interaction had *in vivo* functional significance in a ciliopathy animal model. We determined the phenotypes of zebrafish embryos 72 h post-fertilization (hpf), following knock-down of *mks3* expression (Fig. 5 and Supplementary Material, Figs S5 and S6). The morpholino oligonucleotide targeted an exon–intron splice site (Supplementary Material, Fig. S5A). Direct sequencing (data not shown) and reverse transcription–polymerase chain reaction (RT-PCR) confirmed that the morpholino caused a splicing defect with inclusion of intronic sequence following exon 3 in the mRNA (Supplementary Material, Fig. S5B) and subsequent loss of reading frame and probable protein truncation.

The *mks3* morphant phenotypes closely reiterated those of human MKS, including both mild and severe proximal and distal notochord anomalies, which can extend through the myotome layer and fin to the surface, a feature suggestive of a meningocele and encephalocele (Fig. 5A and Supplementary Material, Fig. S5C, D and I). Additional *mks3* morphant phenotypes included abnormal eye formation, single otic placode, renal cyst formation and dilation of the pronephrotic duct (Supplementary Material, Fig. S5E–I, summarized in Supplementary Material, Fig. S5J). The *mks3* morphant phenotype could be rescued by co-microinjection of capped mRNA for human *MKS3* with the *mks3* morpholino (Fig. 5B and Supplementary Material, Fig. S5K). Higher levels of *mks3* morpholino caused a dose-dependant effect on mortality at 24 hpf (Supplementary Material, Fig. S5L).

The closest zebrafish orthologue of mammalian filamin A is 'actin-binding protein 280' (Zfin gene id: ZDB-GENE-041008-175) and for the purposes of convenience, we label the gene *flna*. To test for possible genetic interaction between *mks3* and *flna*, we first investigated morphants at 72 hpf following *flna* knockdown. At low doses of morpholino oligonucleotides, we saw pronephric cyst formation (Fig. 5C) and other development defects of variable severity (Fig. 5D) including cardiac oedema, hydrocephalus, body axis deformities, in addition to otic placode defects (Supplementary Material, Fig. S6A and B) and eye defects (Supplementary Material, Fig. S6C and D). Higher doses of *flna* morpholino oligonucleotides caused a dose-dependant effect on mortality at 24 hpf (Fig. 3E). Furthermore, the combination of low doses of both *mks3* and *flna* morpholinos produced a statistically significant effect, with increases in both the incidence and severity of developmental defects (severe brain and body axis defects, cardiac oedema, otic placode and eye defects; Fig. 5F and G, Supplementary Material, Fig. S6E) and increased mortality (Fig. 5H).

Loss of filamin A expression in *Flna^{Dilp2}* mouse embryos disrupts meckelin distribution, cilia formation and basal body position

We investigated the distribution of meckelin, cilia formation and basal body positioning in the filamin A null mouse strain *Flna^{Dilp2}* (30). The third, fourth and lateral ventricles of male *Flna^{Dilp2}* hemizygous mouse embryos at E13.5 were highly dysmorphic, with extensive disruption of the ventricular zone of the developing neocortex, particularly the fourth ventricle which was fused with the aqueduct, and the presence of severe oedema (Fig. 6A). In addition, severe PVH was observed in the fourth ventricle and also the third ventricle (Fig. 6A), demonstrating one of the major phenotypes caused by *FLNA* mutation in humans (20) and confirming the *Flna^{Dilp2}* mouse is an appropriate model for this disease.

We next immunostained adjacent transverse sections with the anti-meckelin Ct antibody and examined the ciliated neuroepithelial layers of the lateral and third ventricles. At this stage of development, neuroepithelial cells display a single primary cilium. In the wild-type lateral ventricle, meckelin was clearly seen in a distinct layer at the apical cell surface (Fig. 6B). This is consistent with the apical localization of meckelin seen in IMCD3 cells using higher-resolution confocal microscopy (Fig. 1B). Furthermore, a discrete, punctuate-basal body-like staining pattern was seen in the third ventricle (Fig. 6B). However, in the lateral and third ventricles of the *Flna^{Dilp2}* mouse, meckelin distribution was disrupted and a diffuse pattern was observed. A weaker localization of meckelin at the apical cell surface was seen in the lateral ventricle. However, at the points where PVH was seen, apical meckelin was completely absent (Fig. 6B).

As disruption of ciliogenesis had been observed with *flna* siRNA knockdown and in PVH patient-derived cells with an *FLNA* mutation (Fig. 3), we examined the neuroepithelial layer of the third ventricle for the presence of cilia and position of the basal body. Transverse sections were immunostained with antibodies raised against polyglutamylated tubulin, γ-tubulin and ZO-1, a tight junction marker, and examined using high-resolution confocal microscopy. In *Flna^{Dilp2}* mice, cilia were present, but their length was significantly reduced (Fig. 6C). Basal body position was also disrupted and basal bodies were positioned aberrantly throughout the neuroepithelial layer, whereas in wild-type embryos basal bodies were positioned in a discrete organized layer in relation to the apical surface (Fig. 6C).

Furthermore, the basolateral cell surfaces of the neuroepithelial layer appeared thickened and less organized in the *Flna^{Dilp2}* mice as demonstrated by the pattern of ZO-1 immunostaining (Fig. 6C). Cell shape was irregular and the intensity of ZO-1 immunostaining was variable at the cell cortex. This was suggestive of disorganization of tight junctions and disruption of the actin cytoskeleton, consistent with the expected role of filamin A in mediating actin cytoskeletal organization.

DISCUSSION

Cilia formation is initiated when the mother centriole migrates to the apical cell surface where it matures to form the basal body. This then acts as a template for the cilium which forms via a process known as intraflagellar transport (15). However, for ciliogenesis to occur, the cell must first display polarity to its external environment, a process dependent on actin remodelling (31–34). In addition, an intact actin network at the apical cell surface is vital for centriole migration and docking (35). This indicates that actin-binding

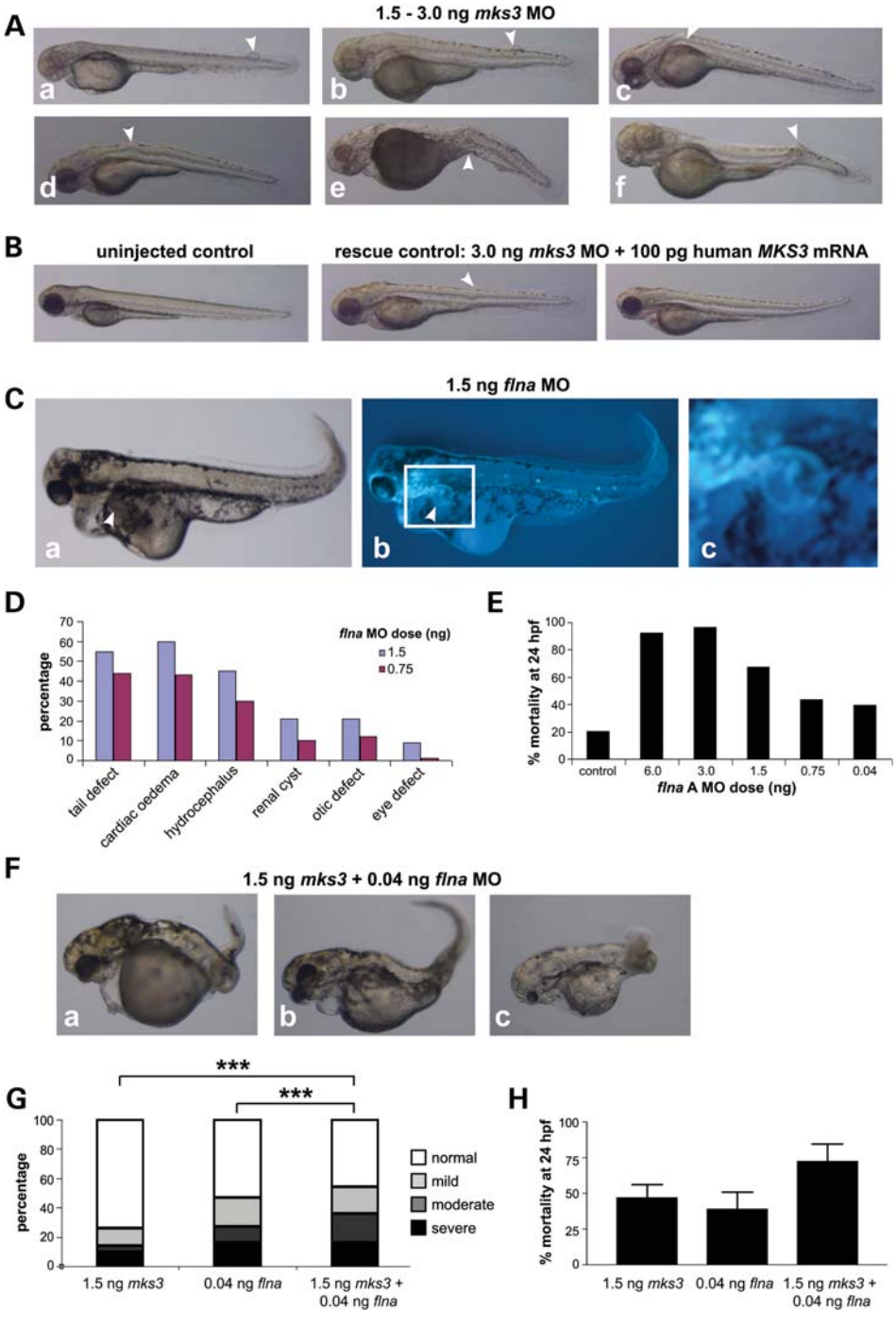

Figure 5. Increases in the severity and incidence of ciliopathy developmental defects in zebrafish embryos following morpholino oligonucleotide knockdown of both *mks3* and *flna* expression. (**A**) Meckelin is required for development of the notochord in zebrafish embryos following morpholino oligonucleotide (MO) knockdown of *mks3* by microinjection at 72 hpf for MO doses 1.5–3.0 ng. Morphant phenotype typical of ciliopathy zebrafish embryo models include (panels a and b) meningocele formation, (c and d) proximal and (e and f) distal notochord abnormalities (arrowheads). (**B**) Normal uninjected control (left panel), and almost complete rescue of the phenotype (middle and right panels) seen with co-injection of human *MKS3* mRNA (100 pg) and *mks3* MO (3 ng dose). A mild notochord defect is indicated (arrowhead). (**C**) Pronephric cyst formation in filamin A (*flna*) MO-injected embryos (1.5 ng dose) at 72 hpf, seen under light (panel a) and fluorescence microscopy (b, in claudin-B-GFP transgenic fish; c indicates magnified inset in white frame). RT-PCR confirmed abnormal splicing of *flna* transcripts (data not shown). (**D**) Percentage incidence and range of morphant phenotypes in *flna* MO-injected embryos (1.5 and 0.75 ng doses) at 72 hpf. Numbers of embryos were 69 for 1.5 ng and 81 for 0.75 ng. (**E**) Dose-dependant effect on mortality at 24 hpf seen with increasing dose (0.04–6 ng) of *flna* MO. Number of embryos: control = 1428; Fil A: 6 ng = 133, 3 ng = 99, 1.5 ng = 428, 0.75 ng = 584, 0.04 ng = 487). (**F**) Combined low doses of *mks3* MO (1.5 ng) and *flna* MO (0.04 ng) produced an increase in frequency and severity of developmental defects with (panel a) severe brain and body axis defects, (b) cardiac oedema, (c) otic placode and eye defects. (**G**) Comparison of morphant phenotype percentage incidences for *mks3* MO only ($n = 248$), *flna* MO only ($n = 129$) and combined *mks3* + *flna* MOs ($n = 94$) at 72 hpf. The *y*-axis represents the percentage of embryos displaying severe (black), moderate (dark grey), mild (light grey) and normal (white) phenotypes. Combined *mks3* and *flna* MO treatments show increases in abnormal phenotypes in embryos surviving to 72 hpf. Statistical significance of pair-wise comparisons are shown ($^{***}P < 0.0001$, χ^2-test). (**H**) Increased mortality with combination *mks3* (1.5 ng) and *flna* (0.04 ng) MO treatments seen at 24 hpf. Error bars indicate SEM.

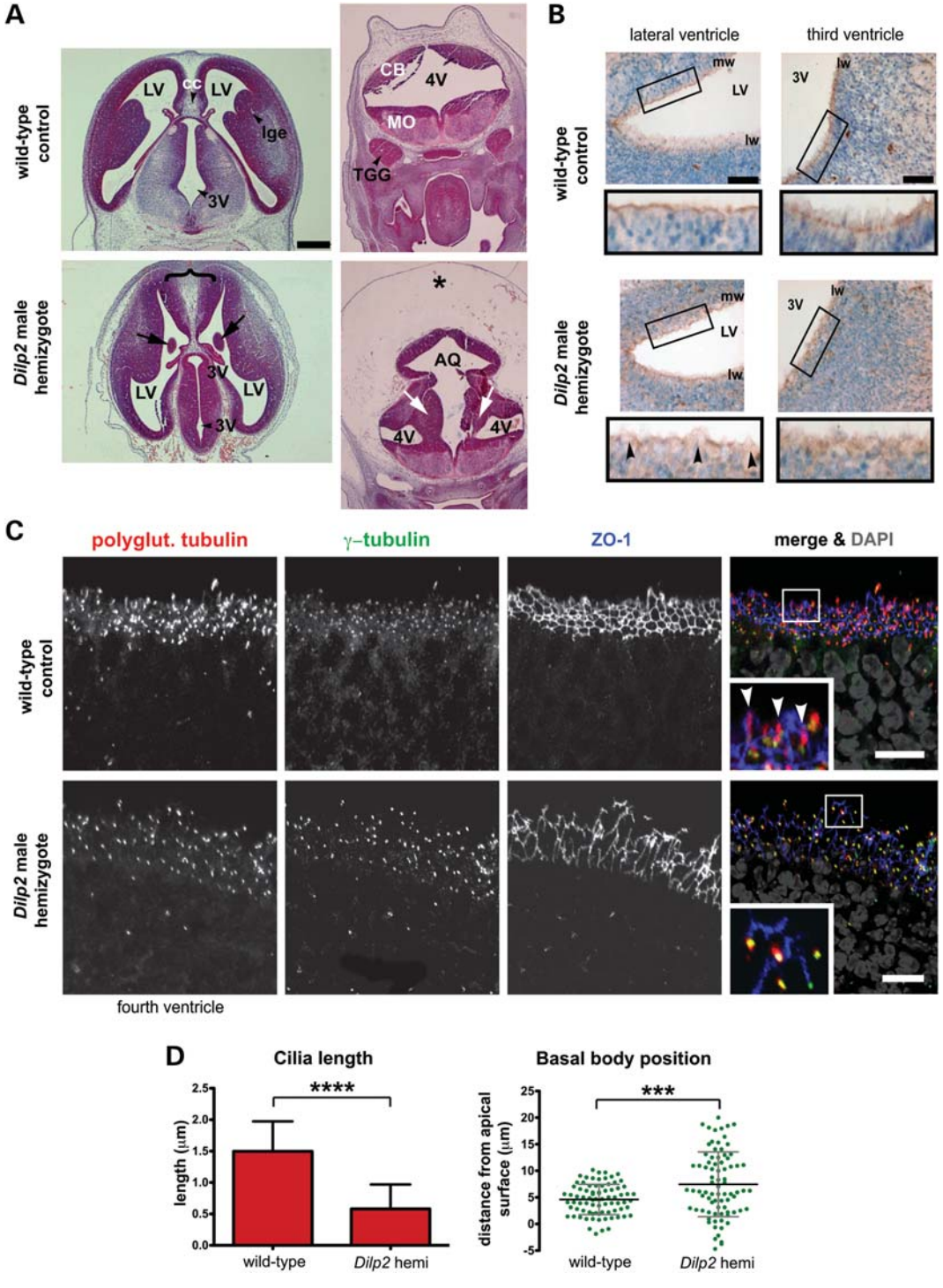

Figure 6. Defects in meckelin localization in neuroepithelial cells of $Flna^{Dilp2}$ E13.5 mouse embryos mutant for filamin A. (**A**) Comparable transverse sections of male wild-type and $Flna^{Dilp2}$ hemizygote embryonic E13.5 brains stained with haematoxylin and eosin, showing normal morphology of the lateral ventricles (LV) and third ventricles (3V) in wild-type controls. The $Flna^{Dilp2}$ brain has a broad mid-line (brace), intraventricular heterotopias (arrows), fusion of the fourth ventricle (4V) with the aqueduct (AQ) and the presence of severe oedema (*). CB, cerebellum; MO, medulla oblongata. Scale bar, 0.3 mm. (**B**) Immunohistochemical staining for meckelin Ct (brown) in neuroepithelial cells of the lateral ventricles (LV; top panels) and third ventricles (3V; bottom panels) for male wild-type matched controls (left-hand panels) and $Flna^{Dilp2}$ (right-hand panels) E13.5 embryo brain sections. Nuclei are stained with Mayer's haematoxylin (blue). Note the diffuse localization of meckelin Ct in $Flna^{Dilp2}$ neuroepithelia (magnified insets in black frames). PVH of neurons is indicated by arrowheads. mw, medial wall, lw, lateral wall. Scale bars, 50 μm. (**C**) Co-immunocytostaining and confocal microscopy of neuroepithelial cells of the third ventricles for adjacent sections to those shown in (B). Stainings are for polyglutamylated tubulin (red), γ-tubulin (green) and ZO-1 (blue) to visualize the cell cortex. The enlarged insets (white border) show cilia in the wild-type controls (arrowheads). Note the disruption of the ZO-1-stained cell cortex in $Flna^{Dilp2}$ mutant cells. Scale bar, 10 μm. (**D**) Upper graph: quantifying cilia length in neuroepithelial cells of the lateral ventricles of male mouse embryo hemizygous for the $Flna^{Dilp2}$ mutation in *Flna*, and male wild-type controls. Mean cilia length was 1.5 μm in wild-type controls and 0.6 μm in $Flna^{Dilp2}$ mutated cells.

proteins have an important role in ciliogenesis and that they may be candidate genes for mutations that result in ciliopathy.

The most severe ciliopathy is MKS, which is caused by mutations in *MKS3/TMEM67*, the gene encoding meckelin (3). Meckelin localizes to the cilium, and we have demonstrated previously an interaction with actin-binding isoforms of nesprin-2 (14). In the present study, we expand the repertoire of actin-binding proteins associated with ciliogenesis and identify a direct interaction of meckelin with filamin A. The filamins are key organizers of the actin cytoskeleton, at the cilium and elsewhere (Fig. 1E and Supplementary Material, Fig. S3E). Our previous work suggested that incorrect remodelling of the actin cytoskeleton is an important pathogenic mechanism for MKS (4,14) and, in the present study, mutation or loss of meckelin expression also led to aberrant actin remodelling. More importantly, we have identified filamins A and B at the basal body and the proximal regions of the cilium where both meckelin and MKS1 co-localize (Fig. 1E and Supplementary Material, Fig. S3C) (**6**), suggesting a role for the filamins at the cilium and the apical cell surface during ciliogenesis.

Actin enrichment at the apical cell surface is necessary for basal body docking (35), and a role for actin-binding proteins during ciliogenesis is supported by a recent reverse genetics siRNA-based screen for modulators of ciliogenesis, which suggested that proteins that regulate actin organization have an the essential role (36). Our studies support this hypothesis and suggest that integrity of the actin cytoskeleton is essential for the correct migration of the centrosome to the apical cell surface prior to ciliogenesis. Knockdown of filamin A expression caused a failure in ciliogenesis and aberrant migration of the centriole pair to the apical cell surface (Fig. 3D and E). Consistent with this observation, PVH fibroblasts with an *FLNA* null mutation also had ciliogenesis and basal body positioning defects (Fig. 3A–C). Finally, hemizygous male mouse embryos for the $Flna^{Dilp2}$ mutation (a null mutation of *Flna*) had both basal body positioning defects and significantly impaired ciliogenesis of neuroepithelial cells in this layer of the neocortex (Fig. 6C and D), because at this stage of development the neuroepithelial cells have a single primary cilium. We therefore speculate that an *in vivo* meckelin–filamin A–actin axis may be essential in mediating basal body migration and docking at the apical cell surface.

The majority of pathogenic mutations in *MKS3* occur in the exons encoding the N-terminal extracellular domain of meckelin (25) and are predicted to be loss of function. In contrast, very few have been noted in the intracellular C-terminal region that interacts with filamin A. We identified an *MKS3* mutation that leads to an in-frame deletion within the C-terminal region of meckelin that interacts with filamin A. Interestingly, the patient in which this mutation was identified had focal glial heterotopias of the cerebellum in addition to the usual clinical features of MKS. Neither glial nor neuronal heterotopia is a common feature of MKS, although an association of nodular heterotopia and encephalocele has been noted previously (37). However, subependymal PVHs and other diverse neuronal migration defects are commonly caused by loss-of-function mutations in *FLNA*, the gene encoding filamin A. We therefore suggest that the manifestation of heterotopia in an MKS-like ciliopathy, and the subsequent *in vitro* analyses of the *MKS3* 919delF mutation, supports our hypothesis that disruption of the meckelin–filamin A interaction can contribute to the ciliopathy phenotype.

To further substantiate the existence of a meckelin–filamin A interaction, we investigated the morphant phenotypes of zebrafish embryos following concurrent knockdown of meckelin and filamin A orthologues using morpholino oligonucleotides. Knockdown of *mks3*, the zebrafish orthologue of human *MKS3*, causes typical ciliopathy developmental defects that include dorsal body axis curvature, renal cysts and otic vesicle anomalies. In keeping with the human MKS phenotype, we observe notochord defects including dorsal extension of the notochord beyond its normal boundary (akin to a meningocele) in *mks3* knockout fish. Therefore, morphant phenotypes closely reiterated the human MKS phenotypes (Fig. 5, Supplementary Material, Figs S5 and S6) and matched the typical pronephric cysts, hydrocephalus and notochord abnormalities typical of perturbed non-canonical (PCP) Wnt signalling defects seen in previous zebrafish models of severe ciliopathies (4,28). PCP mediates many aspects of actin-dependent polarized cell behaviour, including ciliogenesis (31,38,39). Following concurrent knockdown of meckelin and filamin A orthologues in zebrafish, there was a significant increase in the frequency of dysmorphology and severity of the ciliopathy phenotype. This suggests a possible synergistic effect, as there are increases in the severity of all defects previously found in the *mks3* morphant phenotypes and an overall increase in embryonic lethality (Fig. 5F–H).

When we modelled the *MKS3* F919del mutation, the interaction between meckelin and filamin A was lost (Fig. 2C). Further analysis demonstrated this mutation led to defects in ciliogenesis (Fig. 2A and B) and inhibitory effects on normal basal levels of both RhoA activity (Fig. 2D) and canonical Wnt signalling (Fig. 4A). These effects on Wnt signalling could either be direct or indirect through another cellular site or process, but a similar inhibition was also seen following over-expression of filamin A (Fig. 4B). This would suggest that the meckelin–filamin A axis is an important positive modulator of Wnt signalling. However, in contrast, we have shown previously an *MKS3* loss-of-function mutation in the extracellular meckelin domain cause RhoA hyperactivation and morphological defects in cell–cell contacts and the actin cytoskeleton (14), which are reiterated following *Mks3* siRNA knockdown (Supplementary Material, Fig. S2E and F). We therefore suggest that loss-of-function mutations in the meckelin N-terminus would cause deregulation of both RhoA and canonical Wnt signalling, with meckelin acting as a negative modulator of these signalling pathways. In contrast, a mutation in the meckelin C-terminus that abolishes the interaction with filamin A will disrupt a positive modulatory effect on these pathways that is mediated by the meckelin–filamin A axis. In support of this model, filamin A has been shown to

$^{****}P < 0.0001$, Student's *t*-test. Lower graph: quantifying basal body position relative to the apical cell surface (marked by ZO-1 immunostaining) in neuroepithelial cells of the lateral ventricles of a male embryo hemizygous for the $Flna^{Dilp2}$, and male wild-type controls. Basal body position was between −1 and 11 μm in wild-type controls and between −5 and +21 μm in $Flna^{Dilp2}$ mutated cells. $^{***}P < 0.001$, Student's *t*-test.

mediate activation of the Ror2 non-canonical Wnt signalling pathway (27). However, irrespective of whether a meckelin mutation causes Wnt signalling to be deregulated or 'over-regulated', the phenotypic consequence is still the development of the ciliopathy disease state, which is a model supported by previous findings for the pathogenesis of cystic kidney disease (29). Our findings imply that the meckelin–filamin A signalling axis is a key regulator in maintaining correct, normal levels of Wnt signalling.

In summary, this is the first evidence that a pathogenic MKS mutation has a direct biochemical and functional consequence on cell morphology and on Wnt signalling. Our results suggest that meckelin forms a functional complex with filamin A. We speculate that the loss of this interaction through mutation of the meckelin intracellular C-terminus can have similar phenotypic consequences as loss-of-function mutations in filamin A. Furthermore, we suggest that the meckelin–filamin A interaction is essential for the correct migration of the centrosome and the formation of a basal body at the apical cell surface. Our previous work has suggested that the latter process is the key pathogenic event in MKS (6,14) and that deregulation of both RhoA and Wnt signalling occur concurrently with these events (4,14). These pathogenic mechanisms warrant further investigation, because their contribution to the phenotypes of PVH and ciliopathy disease may inform better clinical management of patients and suggest novel therapeutic interventions in the future. However, key questions that remain unanswered is whether the deregulation of Wnt signalling pathways in MKS and other ciliopathies is a direct consequence of ciliogenesis defects, and what role the normal intact cilium has on their regulation.

MATERIALS AND METHODS

Informed consent for use of patients in research

Informed consent was obtained from all participating families or patients, with studies approved by the Leeds (East) Research Ethics Committee (REC ref. no. 08/H1306/85) on 4 July 2008.

Animals

The animal studies described in this paper were carried out under the guidance issued by the Medical Research Council in *Responsibility in the Use of Animals for Medical Research* (July 1993) in accordance with Home Office regulations under the Project Licence nos. PPL60/3785 and PPL 60/4010. The $Flna^{Dilp2}$ strain has been submitted to the European Mouse Mutant Archive (http://www.emmanet.org/) strain number EM:00387.

Y2H assays

The C-terminus intracellular domain of human *MKS3* (meckelin Ct, encoding meckelin amino acids D761–Y925; see Fig. 1A and Supplementary Material, Fig. S1A) was cloned into the lexA vector pB27 and screened against a human foetal brain RP1 prey cDNA library. Y2H screens were performed by Hybrigenics SA, Paris, France, as previously described (12,40).

Cloning

Full-length human *MKS3* was cloned into the pCMV-HA vector as described previously (6). The meckelin Ct region, encoding amino acids D761–Y925, was sub-cloned into an enhanced green fluorescent protein-containing vector (pJA1). Mutations were introduced using the QuickChange mutagenesis kit (Stratagene, Stockport, UK). The pGEX6P-1-GST-meckelin Ct construct (encoding amino acids E756–I995) has been described previously (14). *MKS3* open reading frame was also cloned into the pCS2+ vector in order to make RNA for injection into zebrafish embryos. Full-length human *FLNA* was cloned into the pCMV-c myc vector as described previously (27).

Cells

Mouse inner medullary collecting duct (IMCD3) and human embryonic kidney (HEK293) cells were grown in Dulbecco's minimum essential medium/Ham's F12 supplemented with 10% foetal calf serum at 37°C/5% CO_2. The derivation and culture of *Dilp2* mouse embryonic fibroblasts has been described previously (31). Fibroblasts from a normal undiseased control, an MKS patient and a female patient with PVH were immortalized following transduction with an amphotropic retrovirus encoding the hTERT catalytic subunit of human telomerase, and maintained in fibroblast growth medium (Genlantis, Inc., San Diego, CA, USA) supplemented with 0.2 mg/ml geneticin. Patient 186, a compound heterozygote for the *MKS3* mutations (c.623G>T) + (c.755T>C) causing the predicted nonsense and missense mutations (p.R208X) + (p.M252T) has been described previously (14). The female PVH patient had a family history of seizures and carried a heterozygous *FLNA* mutation c.1587delG, causing the frameshift p.K526fs in filamin A. For the analysis of centrosome positioning and cell migration assays, cells were grown on Transwell permeable supports (Corning, Inc., Amsterdam, The Netherlands).

Antibodies

The following primary antibodies were used: mouse anti-HA clone HA-7, mouse anti-c myc clone 9E10, mouse anti-acetylated-α-tubulin clone 6-11B-1., rabbit anti-HA (Sigma-Aldrich Co. Ltd., Dorset, UK); mouse anti-polyglutamylated tubulin clone GT-335 (Enzo Life Sciences Ltd., Exeter, UK); rabbit anti-GFP ('Living Colors A.v. Peptide Antibody', Clontech, Inc., CA, USA); rabbit anti-filamin A, rabbit-anti-γ-tubulin, mouse anti-β actin clone AC-15 (Abcam Ltd., Cambridge, UK); mouse anti-filamin A clone 4E10-1B2, rabbit anti-filamin B (Abnova Corp., Taipei City, Taiwan); mouse anti-ZO-1, mouse anti-myosin IIB (clones R26.4C and CMII 23, Developmental Studies Hybridoma Bank, University of Iowa, USA); mouse anti-RhoA (Cytoskeleton, Inc., Denver, CO, USA). Rabbit anti-MKS1 and rabbit anti-meckelin C-terminus (meckelin Ct, 'Ct Ab' in Fig. 1A), raised against amino acids 982–995, have been described previously (6). Rabbit anti-meckelin N-terminus (Meckelin Nt, 'Nt Ab'), raised against amino acids 90–103, has also been described (12). Secondary antibodies were Alexa-Fluor 488-, Alexa-Fluor 594- and Alexa-Fluor 568-conjugated goat anti-mouse IgG and goat anti-rabbit

IgG (Life Technologies Corp., NY, USA). Alexa-Fluor 633 phalloidin conjugate (Life Technologies Corp.) was used to visualize F-actin.

Immunoprecipitation, WCE preparation and western blotting

Rabbit antisera were precipitated with 50% (w/v) ammonium sulphate pH 7 and affinity-purified as described previously (41). Co-IP was performed essentially as described previously (41). WCEs containing total soluble proteins were prepared from confluent untransfected HEK293 cells, or IMCD3 cells that had been transiently transfected with 1 μg plasmid constructs in 90 mm tissue culture dishes, or scaled down as appropriate. WCE supernatants were processed for IP experiments by using 5 μg affinity-purified mouse MAbs, or 5–10 μg purified IgG fractions from rabbit polyclonal antisera, coupled to protein G- and/or protein A-sepharose beads (GE Healthcare UK Ltd).

Immunoprecipitates or 10 mg WCE total soluble protein was analysed by sodium dodecyl sulphate—polyacrylamide gel electrophoresis (using 4–12% acrylamide gradient gels) and western blotting according to standard protocols using either rabbit polyclonal antisera (final dilutions of ×200–1000) or MAbs (×1000–5000). Appropriate horseradish peroxidase (HRP)-conjugated secondary antibodies (Dako Ltd., Ely, UK) were used (final dilutions of ×10 000–25 000) for detection by the enhanced chemiluminescence 'Femto West' western blotting detection system (Thermo Fisher Scientific Ltd., Cramlington, UK)

GST pull-down and RhoA activation assays

GST fusion protein GST-meckelin Ct (encoding amino acids 756–986) was purified and used for GST pull-down assays as described previously (14). The activated GTP-bound isoform of RhoA was specifically assayed in pull-down assays using a GST fusion protein of the Rho effector rhotekin (Cytoskeleton, Inc.), using conditions recommended by the manufacturers. WCEs were processed as rapidly as possible at 4°C, and snap-frozen in liquid nitrogen. Total RhoA (in WCEs) and pull-down protein were immunodetected on western blots using a proprietary anti-RhoA MAb (Cytoskeleton, Inc.). Immunoblotting for total RhoA and β-actin was used as loading controls.

Canonical Wnt activity (Topflash) luciferase assays

For luciferase assays of canonical Wnt activity, we grew fibroblasts in 12-well plates and co-transfected with 0.5 μg of Topflash firefly luciferase construct (or Fopflash, as a negative control), 0.5 μg of expression constructs (pCMV HA-meckelin, pCMV c myc-filamin A or empty pCMV-HA/pCMV c myc vector) and 0.1 μg of pRL-TK (Promega Corp., WI, USA; *Renilla* luciferase construct used as an internal control reporter). Cells were treated with Wnt3a- or Wnt5A-conditioned media to stimulate or inhibit the canonical Wnt pathway. We obtained Wnt3A- or Wnt5A-conditioned media from stably transfected L cells with Wnt3A or Wnt5A expression vectors and used as described (42). Control media was from untransfected L cells. Activities from firefly and *Renilla* luciferases were assayed with the Dual-Luciferase Reporter Assay system (Promega Corp.) on a Mithras LB940 (GmbH & Co. KG, Bad Wildbad, Germany) fluorimeter. Minimal responses were noted with co-expression of the Fopflash negative control reporter construct (Supplementary Material, Fig. S10B). Raw readings were normalized with *Renilla* luciferase values. Results reported are from at least four independent biological replicates.

Transfection and siRNA

For transfection with plasmids, cells at 80% confluency were transfected using Fugene 6 (Roche Products Ltd., Welwyn Garden City, UK) according to the manufacturer's instructions and as described previously (14). For RNAi knock-down, siRNA duplexes were designed against mouse *Flna* sequence using Dharmacon's custom SMARTpool siRNA service (Thermo Fisher Scientific Ltd.). Antisense sequences were as follows. *Flna:* duplex 1, 5′-CAGAGUAACAGGUGACGAU; duplex 2, 5′-GCUCAGAGGUAGACGUGGA. *Mks3* siRNA duplexes have been described previously (12). The medium or low-GC non-targeting scrambled siRNA duplexes (Invitrogen) were used as negative controls. siRNAs were pooled, and 100 pmol of each pool was transfected into IMCD-3 cells at 60–80% confluency using Lipofectamine RNAiMax (Life Technologies) and as described previously (4).

Immunohistochemistry

Mouse embryos (embryonic age E13) were fixed in 4% (w/v) paraformaldehyde and embedded in paraffin. Thin sections (4 mm) were cut into slides, deparaffinized and rehydrated using standard methods. Epitope recovery was obtained through boiling in 1 mM ethylenediaminetetraacetic acid, pH 8.0, for 15 min followed by 30 min cooling. Blocking and application of primary antibodies was as described (6). Appropriate HRP-conjugated secondary antibodies (Dako, Inc.) were used (final dilutions of ×10 000–25 000). Sections were developed in 'Sigma Fast' 3,3′-diaminobenzidine with $CoCl_2$ enhancer and counterstained with Mayer's haematoxylin (Sigma-Aldrich Co. Ltd).

Immunofluorescence/confocal microscopy and measurement of cilia length

Cells were seeded at 20×10^3 cells/well on glass coverslips in 6-well plates and fixed in ice-cold methanol (5 min at 4°C) or 2% paraformaldehyde (20 min at room temperature). Permeabilization, blocking methods and immunofluorescence staining were essentially as described previously (4). Primary antibodies were used at final dilutions of ×200–1000. Secondary antibodies and phalloidin conjugate were diluted at ×500. Confocal images were obtained using a Nikon Eclipse TE2000-E system, controlled and processed by EZ-C1 3.50 (Nikon UK Ltd., Kingston Upon Thames, UK) software. Images were assembled using Adobe Illustrator CS2. Cilia length was measured in immunostained histological sections using the 'measurement' tool in the EZ-C1 3.50 (Nikon, Inc.) confocal software. Briefly, a z-stack was taken

through the histological section, and a three-dimensional image rendered using the 'image render' tool in the confocal software. Cilia length was then measured along the long axis of the cilium.

Zebrafish embryo morphant phenotypes

To knockdown *mks3* and/or *flna* in zebrafish, the following morpholino antisense oligonucleotides (MOs) 5′-GTAAAA ATGACAAGCGCCTACCCAG-3′ targeting *mks3* and 5-CC GATTCACCTGAGAGAGGAGAGAC-3′ targeting *flna* (Gene Tools, Inc., Philomath, OR, USA) were microinjected into one–two-cell stage embryos, collected from pairing of zebrafish stocks (Golden/Claudin-b-GFP). The mRNA encoding full-length human *MKS3* was co-injected where indicated. For assessment of morphant phenotypes, live embryos were scored at 24–72 hpf, with 80–100 embryos per injection. If anatomical structures were entirely normal for developmental stage, then they were assigned 'normal'. If there was either a slight variation in morphology suggestive of a developmental delay or a single structural abnormality (e.g. tail defect or slight hydrocephalus), then the phenotype was assigned 'mild'. If the morphant displayed more dysmorphic features together with structural abnormalities, then the phenotype was assigned to be 'moderate' and if the morphant had multiple abnormalities, then it was assigned to be 'severe'. These morphological phenotypes were quantified under bright-field and fluorescence microscopy and based on typical ciliary defects (hydrocephalus, cardiac oedema, notochordal defects and tail defect) or embryonic lethal phenotypes.

SUPPLEMENTARY MATERIAL

Supplementary Material is available at *HMG* online.

ACKNOWLEDGEMENTS

We thank A. Monk, K. Passam and T. Simpson of Nikon UK Ltd for technical support and advice on confocal microscopy, and Lisa McKie for technical assistance. We thank R.T. Moon at the Department of Pharmacology, University of Washington, for the Topflash and Fopflash constructs, and F. Nakamura at Brigham & Women's Hospital, Harvard Medical School, for the c myc-*FLNA* construct. The anti-MKS1 antibody was a gift from N. Katsanis, Duke University Medical Center.

Conflict of Interest statement: All authors declare no conflict of interest.

FUNDING

We acknowledge funding from the UK Medical Research Council (grant G0700073 to M.A. and C.A.J.), and an Egyptian Government Scholarship (to Z.A.). The research also received funding from the European Community's Seventh Framework Programme FP7/2009 under grant agreement no. 241955 SYSCILIA, the Wellcome Trust (to K.G.), Kidney Research UK (to R.J.S.), a Beit Memorial Fellowship for Medical Research (to H.R.D.), the Royal Society (to H.R.D.) and the E.P. Araham Trust (to H.R.D.). The *Flna*^{Dilp2} mutant was found in an ENU mutagenesis program supported by GlaxoSmithKline.

REFERENCES

1. Baala, L., Audollent, S., Martinovic, J., Ozilou, C., Babron, M.C., Sivanandamoorthy, S., Saunier, S., Salomon, R., Gonzales, M., Rattenberry, E. *et al.* (2007) Pleiotropic effects of CEP290 (NPHP6) mutations extend to Meckel syndrome. *Am. J. Hum. Genet.*, **81**, 170–179.
2. Kyttala, M., Tallila, J., Salonen, R., Kopra, O., Kohlschmidt, N., Paavola-Sakki, P., Peltonen, L. and Kestila, M. (2006) MKS1, encoding a component of the flagellar apparatus basal body proteome, is mutated in Meckel syndrome. *Nat. Genet.*, **38**, 155–157.
3. Smith, U.M., Consugar, M., Tee, L.J., McKee, B.M., Maina, E.N., Whelan, S., Morgan, N.V., Goranson, E., Gissen, P., Lilliquist, S. *et al.* (2006) The transmembrane protein meckelin (MKS3) is mutated in Meckel–Gruber syndrome and the wpk rat. *Nat. Genet.*, **38**, 191–196.
4. Valente, E.M., Logan, C.V., Mougou-Zerelli, S., Lee, J.H., Silhavy, J.L., Brancati, F., Iannicelli, M., Travaglini, L., Romani, S., Illi, B. *et al.* (2010) Mutations in TMEM216 perturb ciliogenesis and cause Joubert, Meckel and related syndromes. *Nat. Genet.*, **42**, 619–625.
5. Roume, J., Genin, E., Cormier-Daire, V., Ma, H.W., Mehaye, B., Attie, T., Razavi-Encha, F., Fallet-Bianco, C., Buenerd, A., Clerget-Darpoux, F. *et al.* (1998) A gene for Meckel syndrome maps to chromosome 11q13. *Am. J. Hum. Genet.*, **63**, 1095–1101.
6. Dawe, H.R., Smith, U.M., Cullinane, A.R., Gerrelli, D., Cox, P., Badano, J.L., Blair-Reid, S., Sriram, N., Katsanis, N., Attie-Bitach, T. *et al.* (2007) The Meckel–Gruber syndrome proteins MKS1 and meckelin interact and are required for primary cilium formation. *Hum. Mol. Genet.*, **16**, 173–186.
7. Delous, M., Hellman, N.E., Gaude, H.M., Silbermann, F., Le Bivic, A., Salomon, R., Antignac, C. and Saunier, S. (2009) Nephrocystin-1 and nephrocystin-4 are required for epithelial morphogenesis and associate with PALS1/PATJ and Par6. *Hum. Mol. Genet.*, **18**, 4711–4723.
8. Arts, H.H., Doherty, D., van Beersum, S.E., Parisi, M.A., Letteboer, S.J., Gorden, N.T., Peters, T.A., Marker, T., Voesenek, K., Kartono, A. *et al.* (2007) Mutations in the gene encoding the basal body protein RPGRIP1L, a nephrocystin-4 interactor, cause Joubert syndrome. *Nat. Genet.*, **39**, 882–888.
9. Vierkotten, J., Dildrop, R., Peters, T., Wang, B. and Ruther, U. (2007) Ftm is a novel basal body protein of cilia involved in Shh signalling. *Development*, **134**, 2569–2577.
10. Bergmann, C., Fleigauf, M., Bruchle, N.O., Frank, V., Olbrich, H., Kirschner, J., Schermer, B., Schmedding, I., Kispert, A., Kranzlin, B. *et al.* (2008) Loss of nephrocystin-3 function can cause embryonic lethality, Meckel–Gruber-like syndrome, situs inversus, and renal–hepatic–pancreatic dysplasia. *Am. J. Hum. Genet.*, **82**, 959–970.
11. Shaheen, R., Faqeih, E., Seidahmed, M.Z., Sunker, A., Alali, F.E., AlQahtani, K. and Alkuraya, F.S. (2011) A TCTN2 mutation defines a novel Meckel–Gruber syndrome locus. *Hum. Mutat.*, **32**, 573–578.
12. Baala, L., Romano, S., Khaddour, R., Saunier, S., Smith, U.M., Audollent, S., Ozilou, C., Faivre, L., Laurent, N., Foliguet, B. *et al.* (2007) The Meckel–Gruber syndrome gene, MKS3, is mutated in Joubert syndrome. *Am. J. Hum. Genet.*, **80**, 186–194.
13. Williams, C.L., Li, C., Kida, K., Inglis, P.N., Mohan, S., Semenec, L., Bialas, N.J., Stupay, R.M., Chen, N., Blacque, O.E. *et al.* (2011) MKS and NPHP modules cooperate to establish basal body/transition zone membrane associations and ciliary gate function during ciliogenesis. *J. Cell Biol.*, **192**, 1023–1041.
14. Dawe, H.R., Adams, M., Wheway, G., Szymanska, K., Logan, C.V., Noegel, A.A., Gull, K. and Johnson, C.A. (2009) Nesprin-2 interacts with meckelin and mediates ciliogenesis via remodelling of the actin cytoskeleton. *J. Cell Sci.*, **122**, 2716–2726.
15. Adams, M., Smith, U.M., Logan, C.V. and Johnson, C.A. (2008) Recent advances in the molecular pathology, cell biology and genetics of ciliopathies. *J. Med. Genet.*, **45**, 257–267.
16. Calderwood, D.A., Huttenlocher, A., Kiosses, W.B., Rose, D.M., Woodside, D.G., Schwartz, M.A. and Ginsberg, M.H. (2001) Increased

filamin binding to beta-integrin cytoplasmic domains inhibits cell migration. *Nat. Cell Biol.*, **3**, 1060–1068.
17. Tu, Y., Wu, S., Shi, X., Chen, K. and Wu, C. (2003) Migfilin and Mig-2 link focal adhesions to filamin and the actin cytoskeleton and function in cell shape modulation. *Cell*, **113**, 37–47.
18. Robertson, S.P., Twigg, S.R., Sutherland-Smith, A.J., Biancalana, V., Gorlin, R.J., Horn, D., Kenwrick, S.J., Kim, C.A., Morava, E., Newbury-Ecob, R. *et al.* (2003) Localized mutations in the gene encoding the cytoskeletal protein filamin A cause diverse malformations in humans. *Nat. Genet.*, **33**, 487–491.
19. Feng, Y. and Walsh, C.A. (2004) The many faces of filamin: a versatile molecular scaffold for cell motility and signalling. *Nat. Cell Biol.*, **6**, 1034–1038.
20. Fox, J.W., Lamperti, E.D., Eksioglu, Y.Z., Hong, S.E., Feng, Y., Graham, D.A., Scheffer, I.E., Dobyns, W.B., Hirsch, B.A., Radtke, R.A. *et al.* (1998) Mutations in filamin 1 prevent migration of cerebral cortical neurons in human periventricular heterotopia. *Neuron*, **21**, 1315–1325.
21. Eksioglu, Y.Z., Scheffer, I.E., Cardenas, P., Knoll, J., DiMario, F., Ramsby, G., Berg, M., Kamuro, K., Berkovic, S.F., Duyk, G.M. *et al.* (1996) Periventricular heterotopia: an X-linked dominant epilepsy locus causing aberrant cerebral cortical development. *Neuron*, **16**, 77–87.
22. Ithychanda, S.S., Hsu, D., Li, H., Yan, L., Liu, D.D., Das, M., Plow, E.F. and Qin, J. (2009) Identification and characterization of multiple similar ligand-binding repeats in filamin: implication on filamin-mediated receptor clustering and cross-talk. *J. Biol. Chem.*, **284**, 35113–35121.
23. Vadlamudi, R.K., Li, F., Adam, L., Nguyen, D., Ohta, Y., Stossel, T.P. and Kumar, R. (2002) Filamin is essential in actin cytoskeletal assembly mediated by p21-activated kinase 1. *Nat. Cell Biol.*, **4**, 681–690.
24. Ohta, Y., Hartwig, J.H. and Stossel, T.P. (2006) FilGAP, a Rho- and ROCK-regulated GAP for Rac binds filamin A to control actin remodelling. *Nat. Cell Biol.*, **8**, 803–814.
25. Khaddour, R., Smith, U., Baala, L., Martinovic, J., Clavering, D., Shaffiq, R., Ozilou, C., Cullinane, A., Kyttala, M., Shalev, S. *et al.* (2007) Spectrum of MKS1 and MKS3 mutations in Meckel syndrome: a genotype–phenotype correlation. Mutation in brief #960. Online. *Hum. Mutat.*, **28**, 523–524.
26. Van Aelst, L. and D'Souza-Schorey, C. (1997) Rho GTPases and signaling networks. *Genes Dev.*, **11**, 2295–2322.
27. Nomachi, A., Nishita, M., Inaba, D., Enomoto, M., Hamasaki, M. and Minami, Y. (2008) Receptor tyrosine kinase Ror2 mediates Wnt5a-induced polarized cell migration by activating c-Jun N-terminal kinase via actin-binding protein filamin A. *J. Biol. Chem.*, **283**, 27973–27981.
28. Gerdes, J.M., Liu, Y., Zaghloul, N.A., Leitch, C.C., Lawson, S.S., Kato, M., Beachy, P.A., Beales, P.L., DeMartino, G.N., Fisher, S. *et al.* (2007) Disruption of the basal body compromises proteasomal function and perturbs intracellular Wnt response. *Nat. Genet.*, **39**, 1350–1360.
29. Lancaster, M.A., Louie, C.M., Silhavy, J.L., Sintasath, L., Decambre, M., Nigam, S.K., Willert, K. and Gleeson, J.G. (2009) Impaired Wnt-beta-catenin signaling disrupts adult renal homeostasis and leads to cystic kidney ciliopathy. *Nat. Med.*, **15**, 1046–1054.
30. Hart, A.W., Morgan, J.E., Schneider, J., West, K., McKie, L., Bhattacharya, S., Jackson, I.J. and Cross, S.H. (2006) Cardiac malformations and midline skeletal defects in mice lacking filamin A. *Hum. Mol. Genet.*, **15**, 2457–2467.
31. Park, T.J., Haigo, S.L. and Wallingford, J.B. (2006) Ciliogenesis defects in embryos lacking inturned or fuzzy function are associated with failure of planar cell polarity and Hedgehog signaling. *Nat. Genet.*, **38**, 303–311.
32. Jones, C., Roper, V.C., Foucher, I., Qian, D., Banizs, B., Petit, C., Yoder, B.K. and Chen, P. (2008) Ciliary proteins link basal body polarization to planar cell polarity regulation. *Nat. Genet.*, **40**, 69–77.
33. Gray, R.S., Abitua, P.B., Wlodarczyk, B.J., Szabo-Rogers, H.L., Blanchard, O., Lee, I., Weiss, G.S., Liu, K.J., Marcotte, E.M., Wallingford, J.B. *et al.* (2009) The planar cell polarity effector Fuz is essential for targeted membrane trafficking, ciliogenesis and mouse embryonic development. *Nat. Cell Biol.*, **11**, 1225–1232.
34. Zeng, H., Hoover, A.N. and Liu, A. (2010) PCP effector gene *Inturned* is an important regulator of cilia formation and embryonic development in mammals. *Dev. Biol.*, **339**, 418–428.
35. Pan, J., You, Y., Huang, T. and Brody, S.L. (2007) RhoA-mediated apical actin enrichment is required for ciliogenesis and promoted by Foxj1. *J. Cell Sci.*, **120**, 1868–1876.
36. Kim, J., Lee, J.E., Heynen-Genel, S., Suyama, E., Ono, K., Lee, K., Ideker, T., Aza-Blanc, P. and Gleeson, J.G. (2010) Functional genomic screen for modulators of ciliogenesis and cilium length. *Nature*, **464**, 1048–1051.
37. Roelens, F.A., Barth, P.G. and van der Harten, J.J. (1999) Subependymal nodular heterotopia in patients with encephalocele. *Eur. J. Paediatr. Neurol.*, **3**, 59–63.
38. Veeman, M.T., Axelrod, J.D. and Moon, R.T. (2003) A second canon: functions and mechanisms of beta-catenin-independent Wnt signaling. *Dev. Cell*, **5**, 367–377.
39. Veeman, M.T., Slusarski, D.C., Kaykas, A., Louie, S.H. and Moon, R.T. (2003) Zebrafish prickle, a modulator of noncanonical Wnt/Fz signaling, regulates gastrulation movements. *Curr. Biol.*, **13**, 680–685.
40. Formstecher, E., Aresta, S., Collura, V., Hamburger, A., Meil, A., Trehin, A., Reverdy, C., Betin, V., Maire, S., Brun, C. *et al.* (2005) Protein interaction mapping: a *Drosophila* case study. *Genome Res.*, **15**, 376–384.
41. Johnson, C.A., Padget, K., Austin, C.A. and Turner, B.M. (2001) Deacetylase activity associates with topoisomerase II and is necessary for etoposide-induced apoptosis. *J. Biol. Chem.*, **276**, 4539–4542.
42. Willert, K., Brown, J.D., Danenberg, E., Duncan, A.W., Weissman, I.L., Reya, T., Yates, J.R. III and Nusse, R. (2003) Wnt proteins are lipid-modified and can act as stem cell growth factors. *Nature*, **423**, 448–452.